Journal of ELECTRONIC MATERIALS, Vol. 43, No. 7, 2014
DOI: 10.1007/s11664-014-3176-4

The Effect of Cooling Rate on Grain Orientation and Misorientation Microstructure of SAC105 Solder Joints Before and After Impact Drop Tests

PAYAM DARBANDI,[1,4] THOMAS R. BIELER,[2]
FARHANG POURBOGHRAT,[1] and TAE-KYU LEE[3]

1.—Mechanical Engineering, Michigan State University, East Lansing, MI, USA. 2.—Chemical Engineering and Materials Science, Michigan State University, East Lansing, MI, USA. 3.—Cisco Systems, Inc., San Jose, CA, USA. 4.—e-mail: payamdarbandi@yahoo.com

The effect of different cooling rates on as-assembled Sn1.0Ag0.5Cu (wt.%) solder joints was investigated by using orientation imaging microscopy to characterize evolution of the microstructure and orientation distribution on test samples before and after shock testing. Evolution of the microstructure of joints located near the corners after shock testing differed substantially for samples cooled at different rates after fabrication. After shock and impact testing, much recrystallization was observed for the rapidly cooled samples; this led to polycrystalline microstructures that were effective in absorbing impact energy, by incorporating a growing crack into the recrystallized tin microstructure rather than the lower-energy intermetallic interface, and thus prolonging life. The slowly cooled samples contained large amounts of (301)[$\bar{1}$03] mechanical twins, which also led to an increased number of interfaces that were effective in absorbing energy. The smallest amount of new interface generation after shock testing occurred in the normal cooling rate microstructures, which had the shortest life. Analysis of the crack-propagation paths associated with different cooling rates indicates that development of interfaces from either twinning or polycrystalline microstructure favors crack propagation through the solder rather than the intermetallic layer interface, which toughens the joint.

Key words: Pb free solder, mechanical Shock, recrystallization, Sn orientation, OIM

INTRODUCTION

Portable electronic products are becoming increasingly important in our culture. Mechanical shock resistance during mishandling can substantially affect the reliability of these products. Speed, weight, size, and multifunctionality are increasingly important design constraints for electronic products. The primary source of stress in most electronic products arises from temperature fluctuations produced by internally generated heat dissipation and external operating environments. Reliability of electronic products is, to a large extent, determined by the ability of solder alloys to withstand loading and absorb strain energy during operation. For portable products, especially, occasional mechanical shocks are expected, as a result of mishandling or service conditions, for example electronic systems in a vehicle. Shock tolerance is an important concern in the electronic packaging industry and engineers face the challenge of designing reliable products that are sufficiently rugged.[1–3]

With the recent change to lead-free solder alloys, tin-based solders have replaced leaded solders in most microelectronic systems. Sn–Ag–Cu (SAC)-based solders are widely used in the electronics

(Received December 30, 2013; accepted April 8, 2014; published online May 8, 2014)

assembly industry. The impact resistance of SAC alloys is an important design issue. The performance of SAC305 and SAC405 alloys in drop tests is an order of magnitude poorer than for eutectic Sn–Pb alloys, because of the higher compliance and longer stress relaxation time for SAC alloys after deformation.[4–6] This performance difference arises from the as-solidified polycrystalline microstructure of Sn–Pb eutectic solder joints, which can deform more easily because of grain boundary sliding and the extreme softness of Pb. In contrast, the more anisotropic Sn-based solder alloys are stiffer, stronger, and have hard strengthening phases and large grains with irregular shapes.[7–9]

Increasing drop test reliability by changing the alloy composition is an approach which has been studied in recent years. Liu and Lee[4] showed that Mn can increase drop impact reliability. Suh et al.[5] showed that reducing the Ag content very effectively increases the fracture resistance of SAC alloys under high-strain conditions. The Ag content of SAC solder alloys can be an advantage or disadvantage, depending on the application, package, and reliability requirements, because the best Ag content for drop performance is not necessarily the best for optimum thermal fatigue reliability.[6]

In series of studies by Mattila et al.[10–12] different failure features were observed during shock tests at room temperature and high temperature, by use of a high amplitude, high-frequency, vibration tester. They found that the average number of drops to failure of the boards decreased as the temperature was increased. For Sn0.2Ag0.4Cu, four different fracture modes were observed. If the assemblies were not thermally cycled or annealed, an interfacial failure mode was observed. Interconnections that were thermally cycled before the drop test failed by cracking of the bulk solder or a mixed mode of package-side intermetallic and bulk solder cracking.[11]

Although shock behavior is different from thermal fatigue, there is some similarity between these two phenomena, especially mechanistically. Bieler et al.[8] investigated the effect of recrystallization as an important phenomenon in thermal cycling of SAC305 solder joints. Deformation of Sn differs from common metallurgical processes in that Sn is always in a hot deformation condition in which strain, recrystallization, and recovery all occur concurrently in a manner that depends strongly on local dislocation content. They showed that because recrystallized grains develop during thermal cycling to introduce high-energy (random) boundaries that slide easily, they are very vulnerable to damage nucleation. Nevertheless, grain boundary sliding is an energy-dissipative mechanism that can be beneficial for shock conditions. Thus, because grain boundary sliding involves dislocation absorption and emission at a grain boundary, and because recrystallization is driven by grain boundary migration into regions of higher dislocation density, the interrelationship between recovery and recrystallization is an important factor that determines the process of damage evolution for lead-free solder joints.[7,8]

As discussed by Suh et al.,[5] the drop performance of SAC105 alloy is substantially better than that of SAC405. This improvement is attributed to extrinsic toughening mechanisms as a result of the higher bulk compliance (i.e., low elastic modulus because of the smaller fraction of hard intermetallic precipitates) and the higher plastic energy dissipation (i.e., low yield strength) of the SAC105 alloy. This is attributed to a lower volume fraction of the Ag_3Sn phase in the bulk solder. These arguments imply that improving the ability to dissipate energy will effectively improve the shock performance of a solder alloy. Larger amounts of Ag_3Sn dispersoids in the solders can, however, pin grain boundaries and delay the recrystallization during thermal fatigue which maintains a high fraction of coincidence site lattice (CSL) boundaries that are resistant to cracking and grain boundary sliding.[5] Thus, it is important to identify how stable low-energy (strong) boundaries, and grain boundary sliding and cracking, improve or degrade product lifetimes.

In addition to altering the composition of solders, and thus their ability to absorb the shock energy,[13] other methods can be used to improve the drop impact reliability of SAC solders. In this study, controlling the rate of cooling was examined as a method of enhancing shock performance.[13–15] Although cooling rate effects can beneficially alter strength or toughness, and thus improve the reliability of electronic products, it is also important to investigate how the rate of cooling affects mechanisms of deformation, recovery, recrystallization, and crack nucleation and propagation arising from shock loading.

EXPERIMENTAL PROCEDURES

The 12 × 12 mm^2 CABGA (0.5 mm pitch, 256 IO, 10 mm die size) packages used in this study had electrolytic Ni/Au surface finish with 350 μm Sn-1.0Ag-0.5Cu (wt.%) (SAC105) solder balls. The packages were assembled with SAC 305 paste on eight-layered high-T_g FR4, 93 mil (2.36 mm) shock test board (Fig. 1) with an organic surface preservative (OSP) surface finish and a reflow condition of 1 min above the liquidus with a 245°C peak temperature profile. The as-assembled boards were heated to 160°C for 20 min then cooled at different rates by water quenching, air cooling, and slow furnace cooling (1°C/min).

A high-acceleration shock tester was used to impose repeated shock deformations, as illustrated in Fig. 1. The test boards were screwed on to the drop table at four support pin locations at the corners of the board. This configuration enabled the board to bend downward and upward after impact. This oscillating deflection of the package leads to

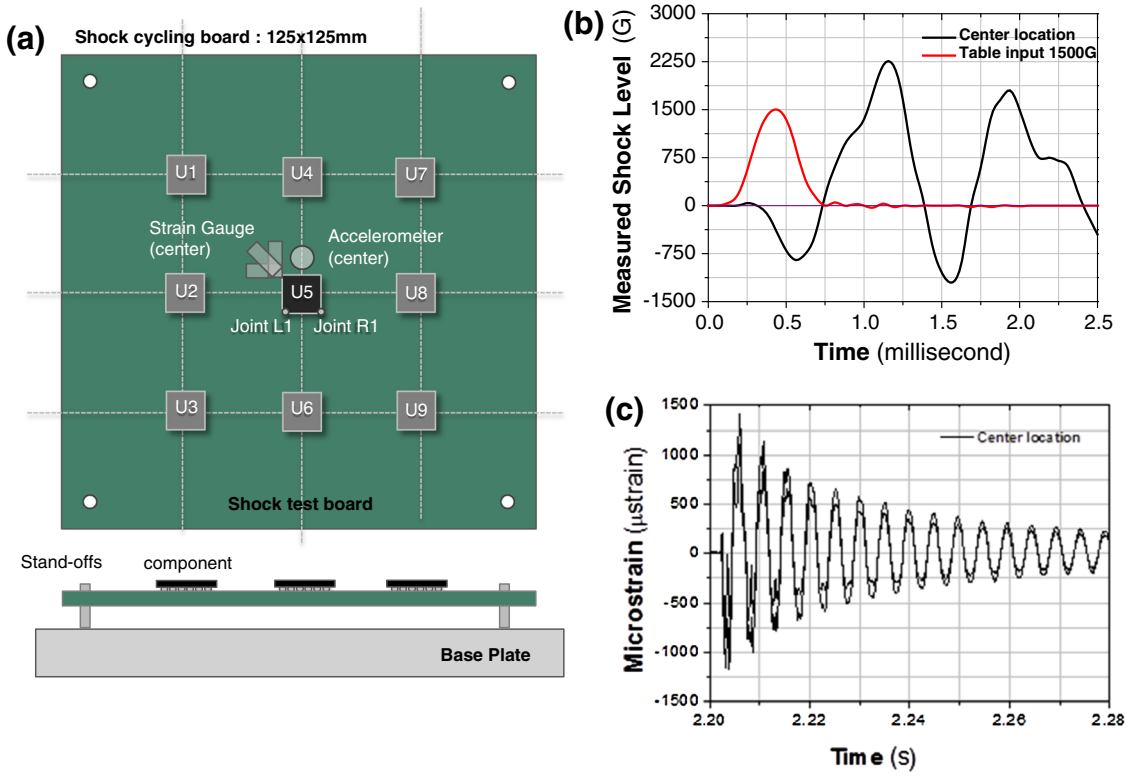

Fig. 1. (a) Shock test board showing the location of packages U1–U9, strain gauges, and accelerometers on the board, and (b, c) examples of shock level and strain from the accelerometer and strain gauges at the center location. The strain plot shows the maximum and minimum strain levels from the three gauges.

opening and closing modes for any crack that forms. The strain was measured by use of three-axis strain gauges 1 mm long; a data-acquisition system was used to collect, record and process the signals. To apply shock loading according to JESD22-B111[3] condition B, the peak G input shock pulse of the drop table was set to impose 1500 G in the form of a half-sine wave with a 0.5-ms period for the package at the center (U5). To satisfy these requirements the drop table was raised and dropped from a calibrated height. When the shock was imposed, the package in the center (U5) experienced the highest shock and strain.

After JESD22-B111, the failure criterion used for this study was a 20% increase in resistance (because the initial resistance was higher than 85 Ω). Eighteen datum points for failure per precondition were collected (from 18 packages on 2 boards), and Weibull statistical analysis was performed to examine the effect of cooling rate on the fracture resistance of solders.[15]

After testing, packages from the center locations were cut from the board, sectioned, mounted, and polished to conduct orientation imaging microscopic (OIM) analysis. The resin surrounding the balls and the package was carefully painted with carbon paint and copper and carbon tape to cover the nonconducting surfaces to prevent the charging effects that cause image distortion or beam drift.

OIM data were obtained by use of an electron microscope with an accelerating voltage of 20 kV and a working distance of 33 mm; a specimen current of approximately 2.4 nA was used to generate electron backscattered diffraction patterns (EBSP). A system with a digiview SEM detector was used. An acquisition speed of 15–20 points per second was obtained by use of a 2 × 2 binning setting. The step size used in this study was 5.0 micron for coarse scans and 0.2 micron for fine scans. OIM analysis software was used to generate the orientation maps. Maps were cleaned by using the neighbor confidence index (CI) correlation to replace pixels that had low CI with their neighbors having a high CI. This step was used to remove minority data points arising from un-indexed or wrongly indexed patterns (e.g. patterns obscured by small Ag_3Sn particles). Grain boundary misorientation statistics were extracted from OIM data, and a user defined c-axis orientation map illustrated in Fig. 2 was used to correlate the orientation of the Sn c-axis relative to the solder–package interface. This c-axis map strategy is effective for visualizing the CTE anisotropy of Sn that was investigated in previous work,[8] and it is also effective for visualizing the elastic anisotropy, because the stiffest direction is along the c-axis, and the most compliant directions are the a-directions, which are easily visualized with overlaid prisms. When the c-axis is parallel to the interface plane,

the orientation is expressed as “red”, and when the c-axis is perpendicular to the surface the orientation is “purple”. Other colors (blue, green, and yellow) fill in the rest of this orientation space.

RESULTS AND DISCUSSION

Initial Microstructure After Different Cooling Rates

Figure 3 shows c-axis maps for five solder joints located on the left side and five joints located on the right side for SAC105 alloys cooled at different rates. Similar to previous studies of SAC alloys, most joints have a single or multi-grained structure with no more than a few Sn grain orientations.[7,8] Irrespective of the cooling rates, there was a combination of single and multi-grained microstructure regions in most joints. Some joints have nearly parallel boundaries in polarized light images (e.g. joint R1 of the slowly cooled sample and L1 of the rapidly cooled sample), which are indicative of mechanical twins observed in samples with different cooling rates (these twins are clearly observed in sample R3 for normal cooling, R1 for slow cooling, and L4 for rapid cooling). Assessment of higher-magnification images revealed twin formation seems to occur more frequently near a free surface than in the sample interior.

During cooling from high-temperature reflow, the package experienced thermal contraction at different rates in different solder joints, which introduced heterogeneous internal stresses. These internal stress states were altered by heating to 160°C and cooling at different rates, leading to different states of internal stored energy. This affected the distribution of single-crystal and multi-crystal joints (Fig. 4); only one single crystal was present after rapid cooling (10%), three were present after slow cooling (30%), and after normal cooling most (70%) of the solder balls were single crystals.

The statistics for grain size and misorientation between grains for each cooling rate are shown in Fig. 5, in which the histograms for all 10 balls using 1° bins are summed then averaged to identify trends. For normal cooling and slow cooling, the misorientation histogram in Fig. 5a contains a high-angle boundary misorientation peak at 62.5°, whereas for rapid cooling two peaks were observed at 58.5° and 61.5° (area A), which are the misorientation angles of {101} and {301} plane twins, respectively. The misorientation data are reported as the total length of a given grain boundary misorientation bin present in a joint, in microns, rather than a normalized value. This approach provides a stereological measure of the grain boundary area (energy) per unit volume that can be quantified and compared with processing history. The twin misorientation boundary length (area) was higher for the rapid and normal cooling conditions. Also, there are more low-angle boundaries under rapid cooling conditions. The grain-size distribution is plotted in Fig. 5b for each case, showing that the slow and normal cooling conditions led to similar distributions, with a large peak at a large grain size. For the rapidly and slowly cooled samples a small population

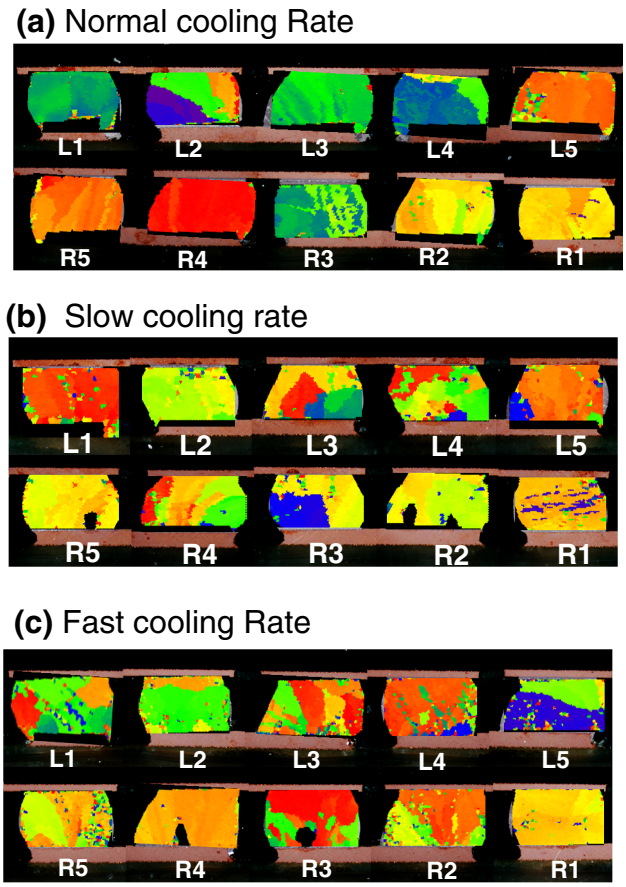

Fig. 3. Cross-section polarized light images and corresponding c-axis maps (relative to the vertical direction) for normally cooled (a), slowly cooled (b), and rapidly cooled (c) samples.

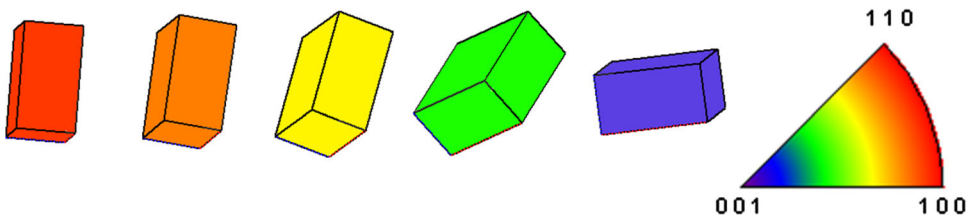

Fig. 2. Sn grain orientation color code used with OIM c-axis maps to identify the c-axis inclination from the interface (Color figure online).

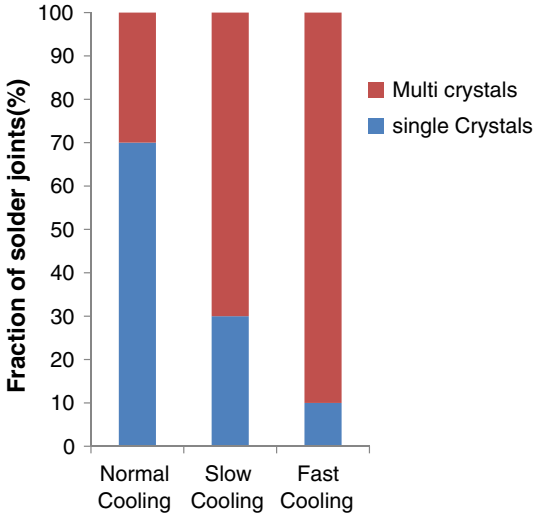

Fig. 4. Fractions of solder joint morphology for different cooling histories.

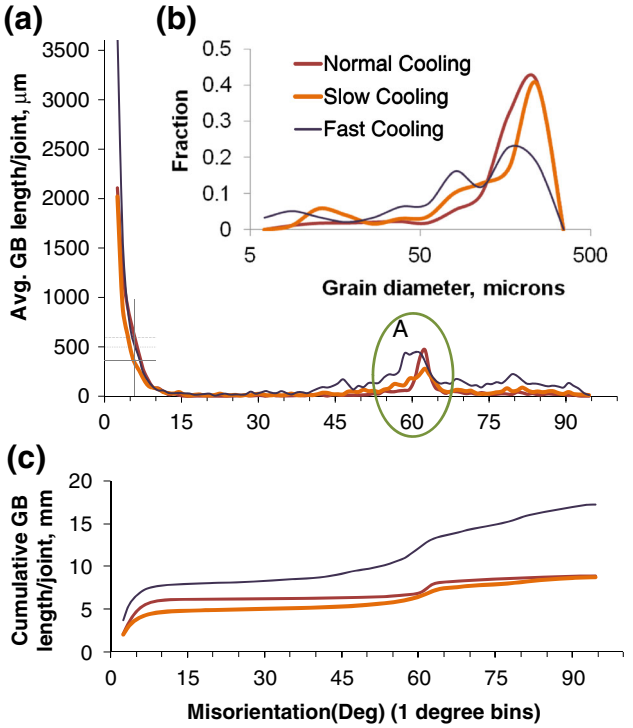

Fig. 5. Misorientation (a), grain diameter (b), and cumulative grain boundary length (c) histograms averaged for the ten solder balls shown in Fig. 3, illustrating low angle boundaries and peaks near 60° associated with solidification twins for normally, slowly, and rapidly cooled samples.

of grains near 10 μm were observed that were absent from the normally cooled sample. The rapidly cooled sample had a lower peak at the largest grain sizes, and several peaks for smaller grain sizes. The *cumulative* grain boundary length in the cross-section is shown in Fig. 5c; this indicates that normal and slow cooling led to the same total boundary length, but the normally cooled sample has more low-angle boundaries. In contrast, the rapidly cooled sample had twice the total length of boundaries. Because of the larger amount of internal energy associated with more grain boundaries, it is evident that rapidly cooled samples have approximately twice the amount of interfacial energy length (area) than the normally and slowly cooled samples.

Microstructure After Shock Testing

Figure 6 shows OIM maps for five joints located on the left and right sides of the package from the boards cooled at different rates and subjected to shock loading. Inspection of each ball revealed cracks in the interfaces which are marked with boxes indicating crack length at the top where interfacial failure was observed and at the bottom where laminate cracking was observed. In contrast with the slowly cooled and normally cooled samples, the OIM images reveal a poly-granular microstructure for rapidly cooled samples (Fig. 6c). These smaller grains are distributed evenly throughout the solder ball cross-section, whereas for slow cooling only a small portion of the cross-section shows fine recrystallized grains, predominantly in the area near the crack (Fig. 5b). Also, twins are observed in joints with different cooling rates after the shock tests; it is not certain whether these are shock-induced twins or whether they were present before shock loading, because twins are also present in samples before shock testing (Fig. 3 L1, L4 for rapidly cooled, R1 for slowly cooled). The effect of shock deformation on the characteristic life for the different cooling rates is shown in Fig. 7; this indicates that the best performance was observed for rapidly cooled polycrystalline samples.

Observation of the highest cumulative length of grain boundaries for rapid cooling (Figs. 4 and 5) indicates that rapid cooling provides the highest amount of total stored energy in these 10 solder balls. This energy can effectively act as a driving force for recrystallization of new grains in the microstructures when additional energy input is added via the shock and the oscillating bending processes after impact. The grain boundary length increases are compared with length before shock in the histograms in Fig. 8. Notably, peaks near the 60° twin misorientations differ substantially depending on previous cooling rate conditions (note that the number of shock cycles for each test differs; Fig. 7). For the rapidly cooled samples there is a large increase in the amount of low-angle sub-grain boundaries between 4° and 15°, and a uniform increase in all other high-angle orientations, which is correlated with a longer life. In contrast, slowly and normally cooled samples change little other than near 60°, which is correlated with a shorter life. The peak for twins near 60° is broadened for

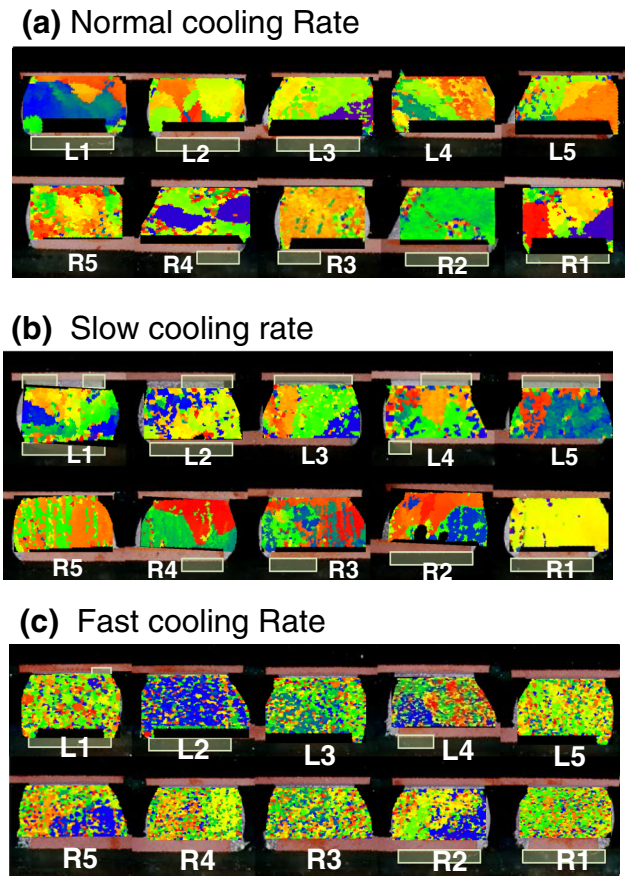

Fig. 6. Cross-section c-axis orientation maps (relative to the vertical direction) after shock tests for normally cooled (a), slowly cooled (b), and rapidly cooled (c) samples. Boxes above and below the joints identify the location of cracks.

both the slowly and normally cooled samples, but the peak is much higher for the slowly cooled sample. This observation shows that the rapidly cooled sample deformed sufficiently to generate new low and high-angle boundaries, and sufficient dislocation content in the form of low angle boundaries to cause these new orientations to grow into neighboring regions with higher defect density (primary recrystallization).[10,16–20] This process led to a large number of grain boundaries.

The presence of mechanical twins in the slowly cooled sample is surprising, and not consistent with conventional wisdom for mechanical twinning, which is expected at high strain and/or low temperatures. However the growth of twins resulting from impact is less surprising, and may have arisen from growth of twins nucleated during slow cooling. The smallest change occurred for the normally cooled sample, with broadening of the twin peak only, indicating that continued deformation led to heterogeneous strain that resulted in spreading of the peak, but because the peak maintained its height, some new twins were also formed. The lack of change is correlated with the shortest lifetime as a result of shock loading.

Figure 9 shows further assessment of the grain boundary statistics presented in Fig. 8, by comparing the three post-shock cases on the same plot in Fig. 9a and the grain size distribution in Fig. 9b. The normally and slowly cooled samples have a grain size distribution similar to that before shock loading, but the original peak at the largest grain size was smaller and a larger, new, peak appeared at a smaller grain size, indicating that the largest grains were subdivided, mostly by twins. In

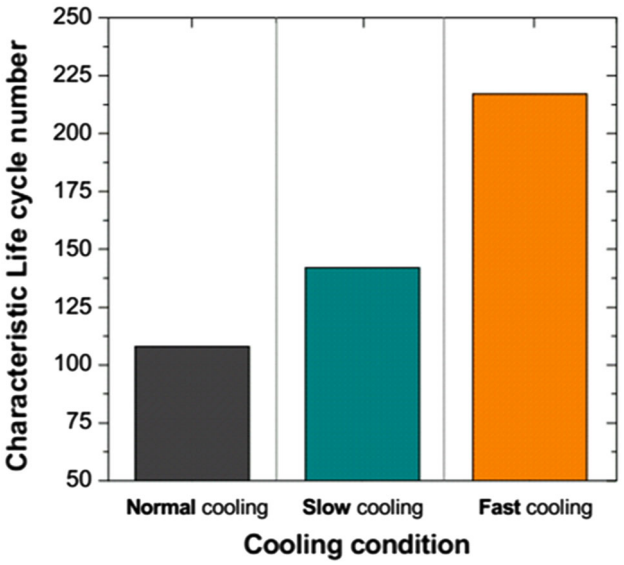

Fig. 7. Characteristic life cycle number after shock tests for different cooling rates.

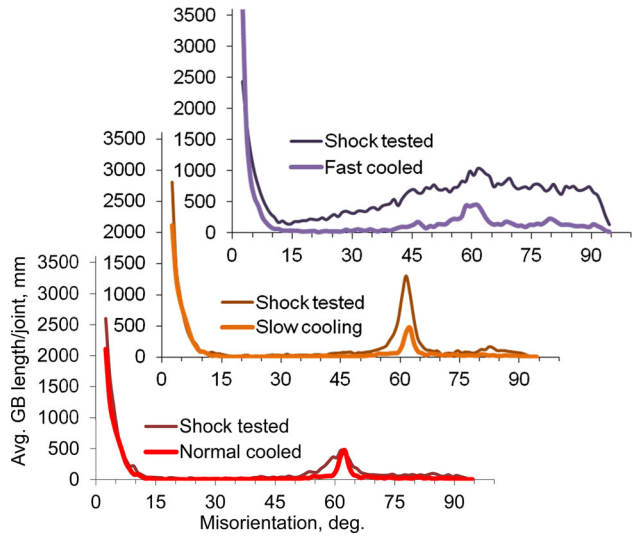

Fig. 8. Comparison of average misorientation histograms before and after shock for the ten solder balls shown in Figs. 3 and 6, illustrating different responses of the microstructure, especially for peaks near 60° associated with solidification twins.

contrast, the shape of the distribution was reversed for the rapidly cooled sample, with a large peak at small grain sizes and smaller peaks for larger grains. The cumulative grain boundary length in Fig. 9c shows that the rapidly cooled samples have 60 mm of grain boundary length per joint, more than three times the amount of length before shock loading, and also more than three times the length observed for normally and slowly cooled samples. The cumulative length increased by ~60% for normal cooling, and ~100% for slow cooling, compared with the cumulative length before shock. To identify the extremes in change, the cumulative grain boundary length for the shocked rapidly cooled samples has 6.4 times the length initially present in the normally or slowly cooled samples.

Because grain boundaries are favored sites for nucleation of recrystallized grains[17], single crystals provide fewer nucleation sites for recrystallization. Critical deformation is necessary to initiate dynamic recrystallization, however.[17] More residual strain is stored in the microstructure produced by rapid cooling, which can assist in providing this critical deformation that enables recrystallization. For the normally and slowly cooled samples, this critical value may not have been reached because of concurrent recovery, except in the localized high-stress areas near the interface where the crack developed. During consecutive shock loading the stored energy and nucleation sites can increase dramatically, and provide energy that can facilitate grain boundary motion needed for recrystallization.

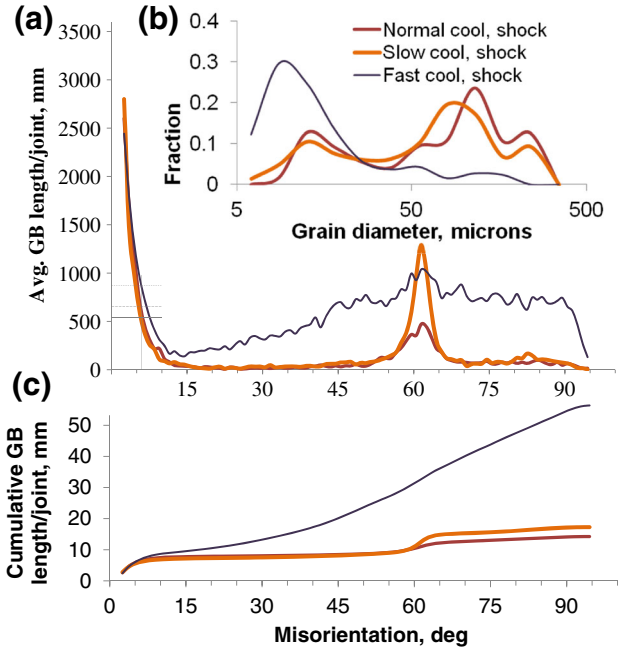

Fig. 9. Comparison of the average misorientation histograms (a) from the ten solder balls shown in Fig. 6. The greatest changes of the averaged grain size histogram (b) and the cumulative boundary length/joint (c) are observed for the rapidly cooled sample.

Figure 10 shows a polarized light image, an SEM micrograph, and c-axis orientation maps for rapidly cooled sample L2 (shown in Fig. 6c). The crack propagation path is evident in the SEM image and the enlarged inset in Fig. 10c. Initiation of the crack occurred at the upper right corner of the solder ball and passed through the Sn phase. With consecutive shock loading, the crack did not travel into the interfacial area. Figure 10d shows that initiation of the crack occurred at a high-angle grain boundary that was not twin-related (not rotated about a [100] axis). The crack propagated diagonally until it ran into a blue oriented grain; this has been observed to be a barrier to crack propagation in thermal cycling studies.[9,21] This crack propagation process is similar to the mechanisms observed in thermomechanically cycled samples.[8]

Figure 11 shows a polarized light image, SEM micrograph, and c-axis map for sample L3 that was initially subjected to slow cooling (Fig. 6b). Similar to rapidly cooled sample L2 in Fig. 10, the crack initiated at the upper right corner of the solder ball. In this case, in contrast with rapid cooling, in which recrystallized grains are observed everywhere in the sample, only the small region near the crack consists of recrystallized grains. It is apparent from Fig. 11c that the initial crack trajectory passed through recrystallized grains but then deflected toward the intermetallic interface. Thus, the grain boundaries in the recrystallized grains were not sufficiently developed to be able to attract the crack, so the crack propagated into and through the interfacial area. The less tortuous crack path in the interface is consistent with a shorter life.

Mechanistic Considerations

These observations of the different evolution of the microstructure in rapidly and slowly cooled samples show that joint lifetime depends on cooling history. During rapid cooling there is greater residual stress and this leads to an increase in the dislocation and vacancy content, increasing the defect energy of the system. Recrystallization is normally not observed at room temperature in SAC joints, because particles pin low and high angle boundaries effectively. However, because room temperature is a high homologous temperature, consecutive shock-loading events can act as an additional force driving recrystallization processes for which there is insufficient thermal activation. The shock and oscillating elastic deformation provide additional energy that can assist recrystallization. The high strain rate deformation can also assist the process by generating new dislocations in most grains, and the subsequent elastic oscillation can act as a catalyst to increase the kinetics of recrystallization during the consecutive loading events. Thus, a shock event can provide new nucleation sites for the recrystallization process, and elastic bending can facilitate boundary

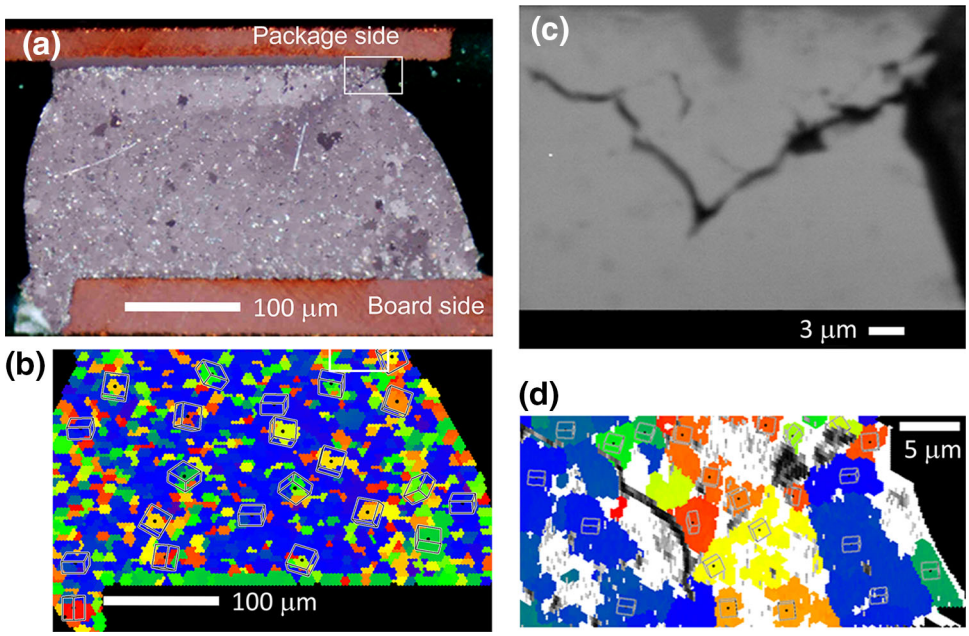

Fig. 10. (a) Polarized light image of cross-section of microstructure for the rapidly cooled and shock tested joint L2. (b) Corresponding c-axis orientation map in the vertical direction and (c) SEM image of enlarged area from the box showing the crack. (d) Corresponding OIM c-axis map with low pattern quality regions overlaid with a gray scale to show the crack-propagation path.

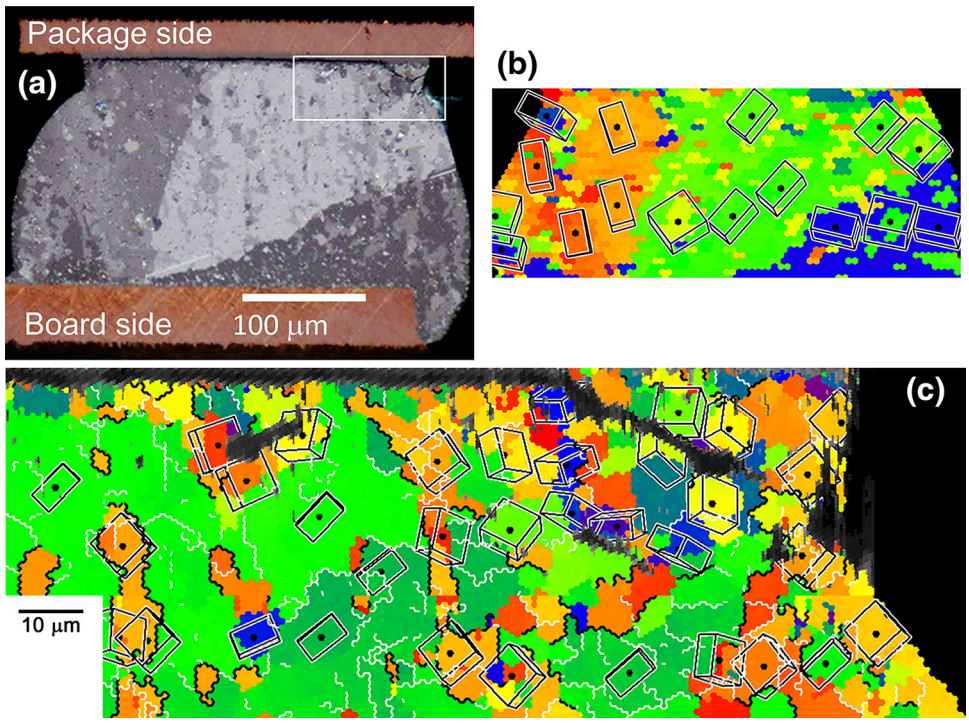

Fig. 11. Polarized light image of cross-section of slowly cooled/shock-tested joint L3 (a) and the corresponding OIM image (b). Orientation map of enlarged area from the box in (a) showing crack and vertical direction c-axis orientation map (c) with overlaid low pattern quality (black and gray regions), showing the location of the crack path in the enlarged area. There is clear evidence of mechanical twins, which are marked with heavy black boundaries (low-angle boundaries are marked in white).

migration. This could account for the poly-granular microstructure that developed in the rapidly cooled shock-tested samples.

During the recrystallization process, internal stress relaxation can also occur; this can substantially alter the crack path. Newly formed grains

have fewer pile-up dislocations and can, consequently, deform with the next impact, and absorb energy. In contrast, with slow or normal cooling, recrystallization was observed mostly in the region near the crack. In this case recrystallization-induced crack propagation caused by generation of weaker high-angle random boundaries can facilitate crack propagation. In contrast, with freshly recrystallized grains and many grain boundaries where sliding can occur to dissipate energy, the impact stress can also generate a large amount of stress, strain, and, hence, dislocation generation leading to rotation, which is evident in c-axis maps. Without uniformly distributed recrystallized grains that are soft and have random high energy boundaries, the solder remains hard, because of pinned low angle (low energy) boundaries, and thus less deformable, leading to load transfer to the board and IMC interface that causes interfacial failure and laminate cracking.[15] Because of the smaller amount of plastic dissipation, the recrystallization process is limited to the region where crack propagation occurs more rapidly, and leads to poorer performance compared with rapid cooling.

CONCLUSIONS

The effect of cooling rate on the shock performance of SAC105 alloy solder joints was investigated quantitatively by using c-axis maps and the statistics of grain boundary evolution. The results reveal a strong effect of cooling rate on the mechanical stability of solder joints during impact. A recrystallization process develops in rapidly cooled samples, because of the greater amount of stored energy; this enables stress relaxation, as a result of sliding on high-energy grain boundaries, which facilitates energy absorption under shock conditions. For normally or slowly cooled samples, the most commonly observed failure mode was a stalled form of recrystallization that facilitated *interfacial* cracking because the unrecrystallized microstructure was unable to attract the crack away from the package-side interface IMC. Newly recrystallized grain boundaries can facilitate grain boundary sliding, which dissipates energy, and further drives recrystallization, which then provides multiple boundaries that can attract cracks away from the IMC layer, making a more tortuous crack path that requires more energy. The more deformable recrystallized microstructure prolongs the lifetime of the joint by preventing load transfer to the IMC interface or the circuit board.

ACKNOWLEDGEMENTS

This work was supported by NSF-GOALI contract 1006656 and Cisco Systems Inc., San Jose, CA, USA.

REFERENCES

1. M. Abtew and G. Selvaduray, *Mater. Sci. Eng. R* 27, 95 (2000).
2. S.K. Kang, P.A. Lauro, D.Y. Shih, D.W. Henderson, and K.J. Puttilitz, *IBM J. Res. Dev.* 49 No. 4/5 July/September 2005.
3. JEDEC Standard JESD22. B111, July 2003.
4. W. Liu and N.C. Lee, *JOM* 59, 26 (2007).
5. D. Suh, D.W. Kim, P. Liu, H. Kim, J.A. Weninger, C.M. Kumar, A. Prasad, B.W. Grimsley, and H.B. Tejada, *Mater. Sci. Eng. A* 460, 595 (2007).
6. D.A. Shnawah, M.F.M. Sabri, and I.A. Badruddin, *Microelectron. Reliab.* 52, 90 (2012).
7. D.W. Henderson, D.E. King, T.M. Korhonen, M.A. Korhonen, L.P. Lehman, E.J. Cotts, S.K. Kang, P. Lauro, D.Y. Shih, C. Goldsmith, and K.J. Puttlitz, *J. Mater. Res.* 19, 1608 (2004).
8. T.R. Bieler, B. Zhou, L. Blair, A. Zamiri, P. Darbandi, F. Pourboghrat, T.K. Lee, and K.C. Liu, *J. Electron. Mater.* 41, 283 (2012).
9. T.K. Lee, B. Zhou, T.R. Bieler, and K.C. Liu, *J. Electron. Mater.* 41, 273 (2011).
10. T.T. Mattila and J.K. Kivilahti, *IEEE Trans. Compon. Packag. Technol.* 33, 629 (2010).
11. T.T. Mattila and J.K. Kivilahti, *J. Electron. Mater.* 35, 250 (2006).
12. T.T. Mattila, P. Marjamäki, and J.K. Kivilahti, *IEEE Trans. Compon. Packag. Technol.* 29, 787 (2006).
13. T.-K. Lee, B. Zhou, T. Bieler, C. Tseng, and J. Duh, *J. Electron. Mater.* 42, 215 (2013).
14. C.-U. Kim, unpublished research.
15. T.-k. Lee, C.-U. Kim, and T.R. Bieler, *J. Electron. Mater.* 43, 69 (2014).
16. M. Ferry and F.J. Humphreys, *Acta Mater.* 44, 1293 (1996).
17. R.D. Doherty, D.A. Hughes, F.J. Humphreys, J.J. Jonas, D.J. Jensen, M.E. Kassner, W.E. King, T.R. McNelley, H.J. McQueen, and A.D. Rollett, *Mater. Sci. Eng. A* 238, 219 (1997).
18. A.U. Telang, T.R. Bieler, A. Zamiri, and F. Pourboghrat, *Acta Mater.* 55, 2265 (2007).
19. H. Chen, J. Han, and M. Li, *J Electron. Mater.* 40, 12 (2011).
20. S. Terashima, T. Kobayashi, and M. Tanaka, *Sci. Technol. Weld. Join.* 13, 732 (2008).
21. B. Zhou, Ph.D. Dissertation, Michigan State University, 2013.